Analysis of Passivated A-286 Stainless Steel Surfaces for Mass Spectrometer Inlet Systems by Auger Electron and X-Ray Photoelectron Spectroscopy and Scanning Electron Microscopy

Henry Ajo*, Donnie Blankenship, Elliot Clark

Savannah River National Laboratory, Savannah River Site, Aiken, South Carolina 29808.

*Corresponding author: Henry.Ajo@srnl.doe.gov 803-725-7649

Abstract

Various commercially available surface treatments are being explored for use on stainless steel components in mass spectrometer inlet systems. Type A-286 stainless steel coupons, approximately 12.5 mm in diameter and 3 mm thick, were passivated with one of five different surface treatments; an untreated coupon served as a control. The surface and near-surface microstructure and chemistry of the coupons was investigated using sputter depth profiling using Auger electron spectroscopy (AES), X-ray photoelectron spectroscopy (XPS), and scanning electron microscopy (SEM). All the surface treatments studied appeared to change the surface morphology dramatically, as evidenced by lack of tool marks on the treated samples in SEM images. In terms of the passivation treatment, Vendors A-D appeared to have oxide layers that were very similar in thickness to each other (0.7-0.9 nm thick), as well as to the untreated samples (the untreated sample oxide layers appeared to be somewhat larger). Vendor E's silicon coating appears to be on the order of 200 nm thick.

Keywords: Tritium, surface passivation, X-ray photoelectron spectroscopy (XPS), Auger Electron Spectroscopy (AES), Scanning Electron Microscopy (SEM), sputter depth profile

Introduction

The surfaces of components of mass spectrometer inlet systems in the Savannah River Site Tritium Facilities are “passivated”. This passivation process prevents impurities in the steel, such as carbon and hydrogen, from entering the gas being analyzed. Stainless steel surfaces can also catalyze gas phase hydrogen isotope exchange and the passivation process likely hinders this catalysis as well [1]. Only two surface passivation vendors are currently used for new components, so it is desirable to seek other commercially available surface treatments that perform as well as the two currently used processes. This paper evaluates four commercial surface treatments different from what is used now; three are specifically stainless steel passivation/electropolishing treatments and the fourth is a chemical-vapor deposited (CVD) silicon coating. Results of testing the gas purity level in containers filled with tritium that were coated using the same five methods and vendors will be reported elsewhere. In the part of this study reported here, flat Type A-286 stainless steel coupons were processed by each of the four candidate passivation or coating treatments, and a fifth coupon using the current vendor’s surface treatment is being characterized as the control. The surface chemical composition was investigated using Auger electron spectroscopy (AES) and X-ray photoelectron spectroscopy (XPS).

Although the stainless steel surface has long been a subject of study [2] due to its technological relevance, the surface passivation of A-286 [3] has not been investigated as extensively as more common stainless steels [2]. A-286 (UNS 66286) (see Table I for composition) is a precipitation-hardenable austenitic stainless steel alloy [4] notable in its difference from the type 304 and 316 stainless steels more commonly used in vacuum

systems, in that the concentration of nickel in A-286 is greater than the concentration of chromium and the nickel content is quite high, 23-25 atomic percent [4]. Another important difference is the presence of 2.2-2.7 atomic percent titanium. In previous work [3] with passivated A-286, titanium was found at the surface in concentrations exceeding its bulk composition. Otherwise, the A-286 sputter depth profile [3] appears qualitatively similar to those seen in 300 series stainless steels [1,3,5-9], with an adventitious carbon layer that is gradually sputtered away and an oxide layer that is indicative of the passivated layer [1,3,5-9]. The oxide layer seen in A-286 in [3] was 4 nm thick. The oxide layer on stainless steels produced by a surface passivation treatment has been shown to be important in reducing the permeability of stainless steels to deuterium and tritium, although the permeability does not necessarily decrease linearly with thickness and the limiting factor seems to be cracks or defects in the oxide layer which allowed some permeability through the stainless steel [3]. The oxide layers for untreated 300 series stainless steels ranged from 1 to 3.5 nm [1,5,6], while the oxide layer for specially treated 300 series stainless steels ranged from 25 nm to 2 microns thick [5-8]. Scanning electron microscopy (SEM) images from the 300 series stainless steels show a relatively smooth and flat untreated surface [1,5,6], except in [7], which shows a relatively rough surface for the untreated stainless steel. However, with passivation treatment, these surfaces become notably rougher [5-7] except for a flow polishing treatment described in [1].

Experimental Procedure

Sample treatments

Type A-286 stainless steel (Table I) coupons, nominally 12.5 mm in diameter and 3 mm thick, were passivated with five different surface treatments: one of the current vendor surface treatments, electropolishing by three different vendors, and a chemical vapor deposited silicon coating.

Depth profiles using Auger electron spectroscopy (AES) and X-ray photoelectron spectroscopy (XPS) were performed on these coupons to characterize the surface and near surface regions. Scanning electron microscope (SEM) images were collected as well using the AES instrument. Since the nature of these surface treatments is proprietary, the vendor treatments are referred to as Vendor A-E.

Instrumentation

A Physical Electronics (PHI) 700NE Nanoprobe was used to perform the depth profiling using AES. SEM images were collected using this instrument as well. The depth profiling was done by sputtering with argon ions at an acceleration voltage of 2.0 keV. AES was done using a 10kV, 10 nA setting on the electron gun and multiplexed collection of the elements of interest. In AES, depth profiles were continued until the composition of the stainless steel surface was constant. SEM image parameters are generally included as part of the image itself-typically the magnification is about 500X.

A Kratos AXIS HSi XPS was used for the XPS measurements. Depth profiling for XPS was done by sputtering using argon ions accelerated to 4.0 keV. XPS was performed using the Magnesium anode at a power of 150 W (15kV, 10mA), and a pass energy of 40 eV. The sputtering rate for AES and XPS was calibrated using a 100 nanometer SiO_2 film on a silicon wafer (Physical Electronics) and measuring the amount of sputter time

required to reduce the oxygen peak to half its maximum value (this is considered sputtering through the film). Consequently, the sputter time in depth profiles are converted to SiO_2 equivalents (in nm) using the sputter rate determined as mentioned above.

All five Vendor samples and the untreated coupon were subjected to AES depth profiling while XPS depth profiles were performed on Vendors B-E only. AES depth profiles were analyzed using Physical Electronics' MultiPak software while XPS depth profiles were analyzed using Kratos' VISION software.

Results and Discussion

Scanning Electron Microscopy (SEM)

In the untreated coupon (Fig. 1), the tooling marks from the machining of the coupon are visible. The surface does not show much heterogeneity with regard to texture or morphology. Also visible is a "raster burn" square due to imaging at higher magnification. Vendor A (Fig. 1) shows a smoother appearance in terms of texture as the tooling marks are no longer visible. Apart from debris visible on the surface, there is very little contrast on the surface, although this may be due to the low accelerating voltage for this image (5.0 kV) compared to that of the untreated surface (20 kV). Vendor B (Fig. 1) shows a fairly smooth surface although the tooling marks are visible as slight contrast. Notable are black areas in the SEM image which are revealed to be composed of carbon by AES. Vendor C (Fig. 1) treatment shows a light threadlike contrast which was not explored for elemental differences. The dark square is "raster

burn" from previous imaging at higher magnification. Vendor D (Fig. 1) shows a mountain range-like morphology, but the AES survey spectra of the two regions was not qualitatively different, and quantitative analysis of the survey spectra indicated that while the elemental composition of the mountain ranges and the smooth surfaces were virtually identical, the "mountains" had more Ca than the smooth surface, while the smooth surface contained more Fe. Vendor E treatment (Fig. 1) shows a bumpy appearance which was not investigated, although it was noted that there was a hole in the surface coating on the coupon (Fig. 2), which revealed the uncoated metal beneath as confirmed by AES survey spectra.

Auger Electron Spectroscopy (AES) depth profiles

An AES survey spectrum of the unsputtered, untreated stainless steel surface is shown in Fig. 3. Before sputtering the surface is seen to be covered by adventitious carbon. Also apparent are O, Fe, and Ni. The untreated surface depth profile in Fig. 4 tracks C, O, Fe, Ni, and Cr. Carbon is present on the surface in all depth profiles. Carbon appearing on the surface of samples exposed to the atmosphere is ubiquitous enough to be referred to as "adventitious carbon". The presence of oxygen is due mainly to surface oxidation of the stainless steel. The oxygen concentration rises to a maximum with depth and then declines continuously. The other components of the stainless steel, Fe, Cr, and Ni, gradually rise throughout the depth profile until they reach steady state values. Another depth profile was taken of another spot on the same untreated sample and it was nearly identical.

The Vendor A depth profile shown in Fig. 5 tracks the same elements as the untreated sample with the addition of Zn, S and Ti. Ti, which is present in the bulk of stainless steel, is present at about 3 atomic % consistently. Zn and S are present in the initial 55 nm of the depth profile. Otherwise, the depth profile of the elements in the treated sample is similar to the untreated sample. The depth profile for Vendor B shown in Fig. 6 tracks the same elements as the untreated sample with the addition of Ti and S. Ti is present throughout the depth profile at about 3%, similar to the Vendor A sample. S appears at about 3% similar to the initial 2 nm of the depth profile. Again, the depth profile of the other elements follows the pattern of the untreated sample. Fig. 7 shows the depth profile of the Vendor C coupon where N appears, rising to 10% by 1 nm and falling down to 4% at 4 nm. Ti is present in the depth profile at about 3 % similar to Vendors A and B surface treatments. The other elements are found to have similar depth profiles as compared to the untreated sample. In the Vendor D coupon shown in Fig. 8, Ca is present at 7% at 1 nm while its concentration drops to 4% at 5 nm and continues to drop. S and Cl were present at < 1% in this sample. Ti is present in the depth profile, < 1% at first, but by 10 nm it is about 3%. The other elements in the sample are found to have similar depth profiles as compared to the untreated sample.

The depth profile for the vendor E coupon shown in Fig. 9 is unlike the other surface treatments as it contains elemental silicon. The depth profile shows a nearly constant Si concentration of 95% for the first 140 nm of the depth profile, after which Si concentration drops and Fe rises, eventually to its bulk values. O rises to a maximum of 25% at about 260 nm after which it drops dramatically. Cr and Ni start to rise at about 160 nm and eventually rise to their bulk values.

Oxide thickness from Auger Electron Spectroscopy (AES) depth profiles

Oxide thicknesses were calculated from the AES depth profiles by taking the difference in depth between the maximum O concentration, labeled Omax (see Table II) and the depth at half the maximum O concentration, labeled Omax/2. The O behavior from the AES depth profiles was used to determine these numbers. Basically, the value of Omax corresponds to the depth at which the O concentration maximized and the Omax/2 is the depth at which the O concentration reached half its maximum value. The difference of these two depths gives an approximate thickness of the oxidation layer, although the results are in nm SiO_2 equivalents, which correspond to the sputtering time. If the ratio of sputtering rates for SiO_2 and the material being sputtered for the conditions in the depth profile are known, the actual physical dimensions of the oxide layer can be calculated [10]. The results in this study are left in dimensions of SiO_2 equivalents, which are reported in nm. These are also the units in which both AES and XPS depth profiles are typically reported.

X-ray Photoelectron Spectroscopy (XPS) depth profiles

Shown following is an XPS survey of the Vendor C treated coupon sputtered down to bulk stainless steel (Fig. 10) as an example of the raw XPS data. The Ni 2p, Fe 2p, Cr 2p, C 1s, O 1s, and Ti 2p peaks were monitored.

Surface treatment by Vendors B, C, D, and E was investigated using XPS depth profiling. Fig. 11 shows the XPS depth profile of the Vendor B sample treatment. As opposed to the AES depth profile, Cr in this depth profile rises to a more or less constant value after the first sputter cycle and stays there. S is not examined in this depth profile. Ti only appears after the first two sputter cycles and then was not present above background. The general pattern for the other elements in the XPS depth profile is similar to that seen for the AES depth profile.

The XPS depth profile of the Vendor C treatment is shown in Fig. 12. Compared to the AES depth profile, the O peak just declines rather than going through a maximum and then declining. Cr also shows a contrasting pattern from the AES profile, rising to a maximum of about 20% after the first sputter cycle and then decreasing eventually to a constant value of 10%. Ti appeared only in the unsputtered sample and after the first two sputter cycles; after that it was not present above background. N was not followed in the XPS depth profile, but the other elements showed similar patterns to the AES depth profile for Vendor C.

The XPS depth profile for Vendor D is shown in Fig. 13. In contrast to the AES depth profile, Ca, Cl, and S were not measured. The Cr behavior in the XPS depth profile shows a peak after the initial sputter cycle and then declines to a constant value of about 10 %. The O does not peak but rather continually declines from 35 % before sputtering to about 10 % after about 5 nm. Ti was not present above background. The other elements in the XPS depth profile behave very similarly to those in the AES depth profile.

The XPS depth profile for Vendor E is shown in Fig. 14. Compared to the AES depth profile, the XPS depth profile did not show S, but otherwise the XPS depth profile is qualitatively very similar to the AES depth profile.

Fig. 15 shows the Cr 2p spectrum as a function of sputter depth in SiO_2 equivalents. XPS reveals the change in oxidation state of the Cr as a function of depth. This allows the identification of at least one constituent of the passivation layer as Cr_2O_3. Clearly at a depth of 0 and 1.2 nm, the positions of the Cr 2p peaks are given by the solid lines. By the 6 nm depth, the Cr 2p peaks have clearly shifted to the positions given by the dashed lines. In between those positions, there appears to be a combination of those peaks. The solid line positions are assigned to Cr_2O_3 while the dashed line positions are assigned to unoxidized Cr metal.

Qualitatively, the AES and XPS depth profiles for Vendors B-E show good agreement with each other for the major elements of interest, which is good for analysis using different techniques on different instruments. Although there are minor differences between the AES and XPS depth profiles, there are several reasons that they are not identical. First of all, our XPS data collection took much longer than AES data collection. As a consequence, fewer XPS data points were taken than the AES data points. Secondly, our XPS instrument had a much larger analysis area, so the depth profile is averaged over a much larger, potentially more heterogeneous area. Finally, the exact same set of elements were not followed in the XPS and AES depth profiles, due in part to the longer data acquisition times for XPS. The atomic % numbers for both depth profiles are based on the set of elements followed and add up to 100%, so inclusion of differing elements will change the atomic % numbers in the different depth profiles.

X-ray Photoelectron Spectroscopy (XPS) thickness calculations

Calculations were performed on the Vendor B, C, and D samples using the XPS MultiQuant software package [11] and the XPS data to determine the thickness of the Cr_2O_3 layer and the adventitious carbon layer above that. These calculations made several simplifying assumptions: that the surface was perfectly flat, the interface between the layers was atomically sharp, that the composition of each layer is pure, and that there are infinite layers over the analysis area. This model is a good approximation when the film morphology is flat without large features or impurities on the surface. This approximation is more valid for Vendors B and C samples with relatively smooth surfaces compared to the Vendor D sample, with its "mountains". The results are qualitative, as the errors in these calculations are often estimated at 20%. However, these results are in actual physical units of the layers themselves rather than SiO_2 equivalents. The results of these calculations are summarized in Table III.

Conclusions

Morphologically, all of the surface treatments studied here appear to change the surface morphology dramatically, as evidenced by lack of tool marks on the treated samples. Vendors A, B, and C had relatively smooth morphologies, while Vendor D's surface treatment resulted in Ca rich "mountains" on the surface and Vendor E's treatment resulted in a bumpy surface that included at least one area that was missing from the coating, leaving the stainless steel exposed. It should also be noted that Vendor B's

treatment appeared to leave large amounts of carbon on the surface, as evidenced by SEM (Fig. 4) and XPS calculations of adventitious carbon thickness (Table III). In marked contrast, Vendor C's treatment resulted in very low amounts of carbon on the surface as evidenced by the AES depth profile (Fig. 7) and XPS calculations of adventitious carbon thickness (Table III). An additional difference between Vendor C's treatment and the other vendors was the presence of nitrogen in the passivation layer which appears to follow the depth profile of oxygen in the passivation layer (see Fig. 7). In terms of the passivation treatment, Vendors A-D appeared to have oxide layers that were very similar in thickness to each other as well as the untreated samples (Table II and Table III); although the untreated sample oxide layers appeared to be larger. Using the method used to determine the oxide thickness in our Auger depth profile, an Auger depth profile of the oxide layer from another study (Fig. 3 in [3]) using modified A-286 stainless steel appears to be roughly 2.5 nm, which is in reasonable agreement with our results. The passivated A-286 appears to have an oxide thickness more in line with the oxide layer on untreated 300 series stainless steels which range from 1 to 3.5 nm [5-7] rather than the 25 nm to 2000 nm [6-9] thick oxide layers observed for specially treated 300 series stainless steels. Vendor E's silicon coating appears to be on the order of 200 nm SiO_2 equivalents thick. In terms of the chemistry of the coatings, they also appear very similar with some elements found in some AES depth profiles at very low concentrations that do not appear in others. However, at those low concentrations, these differences could be a result of sample handling.

The argon ion sputtering rate in our Auger depth profile experiments for the passivation layer appears to be about 50% that of SiO_2, by comparison of the Auger depth profile

results of roughly 2 nm thick with the XPS passivation layer thickness calculations which are roughly 1 nm thick. A study shows that Cr_2O_3 has roughly 50% argon ion sputter rate compared to SiO_2 [10]. This is consistent with the use of Cr_2O_3 as a simple model of the passivation.

In conclusion, to predict performance of these passivation treatments, a relatively simple question should be asked: does the passivated surface show evidence of something other than a clean, smooth passivation layer? From the data, passivation treatments from Vendors B, D, and E appear ineffective due to high carbon contamination, a rough surface contaminated with calcium, and a passivation treatment that left large parts of the surface unpassivated, respectively. In contrast, passivation treatments from Vendors A and C show low carbon contamination, a smooth surface, and complete passivation of the surface. The oxide thicknesses appear similar in the Vendor A-D passivation treatment, so this does not appear to be a differentiating measurement. Finally, containers treated by Vendors A and C are predicted to be the most effective for stably storing Tritium and for Tritium service use in mass spectrometer systems.

Acknowledgements

Brian Stromeyer provided useful discussion. This work was funded by a Plant Directed Research and Development grant.

References

[1] J.T. Gill, W.E. Moddeman, R.E. Ellefson, Chemically Polished Stainless Steel Tubing for Tritium Service Journal of Vacuum Science and Technology A **1**, 869-873 (1983).

[2] R. O. Adams, A Review of the Stainless Steel Surface Journal of Vacuum Science Technology A **1**, 12-18 (1983).

[3] W. A. Swansinger and R. Bastasz, Tritium and Deuterium Permeation in Stainless Steels Influence of Thin Oxide Films Journal of Nuclear Materials **85 & 86**, 335-339 (1979).

[4] PJ. R. Davis, ASM Handbook, Volume 5, Surface Engineering, ASM International, 1994.

[5] A. Vesel, M. Mozetic, A. Drenik, N, Hauptman, M. Balat-Pichelin, High temperature oxidation of stainless steel AISI316L in air plasma Applied Surface Science **255**, 1759 -1765 (2008).

[6] P. Stefanov, D. Stoychev, M. Stoycheva, A. R. Gonzalez-Elipe, Ts. Marinova, XPS, SEM and TEM characterization of stainless-steel 316L surfaces after electrochemical etching and oxidizing Surface and Interface Analysis **28**, 106-110 (1999).

[7] D. Mandrino, M. Godec, M. Torkar, M. Jenko, Study of oxide protective layers on stainless steel by AES, EDS and XPS, Surface and Interface Analysis **40**, 285-289 (2008).

[8] P.V. A. Ignatova, St. Van Dyck, R. Grotzschel, W. Moller, XPS depth profiling of oxide scales of stainless steels formed in high-temperature aqueous conditions, Surface and Interface Analysis **38**, 396-400 (2006).

[9] T. Hryniewicz, K. Rokosz, R. Rokicki, Electrochemical and XPS studies of AISI 316L stainless steel after electropolishing in a magnetic field, Corrosion. Science **50**, 2676-2681 (2008).

[10] D. R. Baer, M. H. Engelhard, A. S. Lea, P. Nachimuthu, T. C. Droubay, J. Kim, B. Lee, C. Mathews, R. L. Opila, L. V. Saraf, W. F. Stickle,R. M. Wallace, B. S. Wright, Comparison of the sputter rates of oxide films relative to the sputter rate of SiO2, Journal of Vacuum Science Technology A **28**, 1060-1072 (2010).

[11] XPS MultiQuant is available at: http://aki.ttk.mta.hu/XMQpages/XMQhome.htm as is the User's manual which explains the calculations in good detail.

Figure Captions

Fig. 1. Scanning electron microscope (SEM) images of untreated stainless steel coupon, and Vendor A-E coupons.

Fig. 2. Scanning electron microscope (SEM) image of Vendor E coupon showing chipped surface.

Fig. 3. Auger electron spectroscopy (AES) survey of the untreated stainless steel surface.

Fig. 4. Auger electron spectroscopy (AES) depth profile of stainless steel blank.

Fig. 5. Auger electron spectroscopy (AES) depth profile of Vendor A treatment.

Fig. 6. Auger electron spectroscopy (AES) depth profile of Vendor B coupon.

Fig. 7. Auger electron spectroscopy (AES) depth profile of Vendor C coupon.

Fig. 8. Auger electron spectroscopy (AES) depth profile of coupon treated by Vendor D.

Fig. 9. Auger electron spectroscopy (AES) depth profile of coupon treated by Vendor E.

Fig. 10. X-ray photoelectron spectroscopy (XPS) survey of Vendor C coupon sputtered down to bulk stainless steel.

Fig. 11. X-ray photoelectron spectroscopy (XPS) depth profile of Vendor B treatment.

Fig. 12. X-ray photoelectron spectroscopy (XPS) depth profile of Vendor C treatment.

Fig. 13. X-ray photoelectron spectroscopy (XPS) depth profile of Vendor D treatment.

Fig. 14. X-ray photoelectron spectroscopy (XPS) depth profile of Vendor E treatment.

Fig. 15. X-ray photoelectron spectroscopy (XPS) depth profile of Vendor treated coupon showing change from Cr_2O_3 to Cr metal.

Tables

Table I. A-286 Nominal Stainless Steel Composition

Element	Min-Max Weight %	Min-Max Atomic %
Nickel	24.00-27.00	22.89-25.32
Chromium	13.50-16.00	14.54-16.94
Titanium	1.90-2.35	2.22-2.70
Manganese	0-2.00	0-2.00
Silicon	0-1.00	0-1.96
Molybdenum	1.00-1.50	0.58-0.86
Vanadium	0.10-0.50	0.11-0.54
Aluminum	0-0.35	0-0.71
Carbon	0-0.08	0-0.37
Phosphorus	0-0.04	0-0.07
Sulfur	0-0.03	0-0.05
Boron	0.001-0.01	0.01-0.05
Iron, Remainder	59.50-49.13	59.65-48.43

Table II. AES depth profile oxide thickness calculation

Sample	Omax (nm)	Omax/2 (nm)	Thickness (nm)
Untreated 1	2	6	4
Untreated 2	2	4.7	2.7
Vendor A	1.5	3.7	2.2
Vendor B	1.3	3.6	2.3
Vendor C	0.6	3.1	2.5
Vendor D	0.9	3.2	2.3

Table III. Calculated adventitious carbon and Cr_2O_3 thicknesses for Vendors B, C, and D.

Sample	Thickness Adventitious Carbon (nm)	Thickness Cr_2O_3 (nm)
Vendor B	5.6	0.9
Vendor C	1.8	0.9
Vendor D	2.4	0.7

Figures

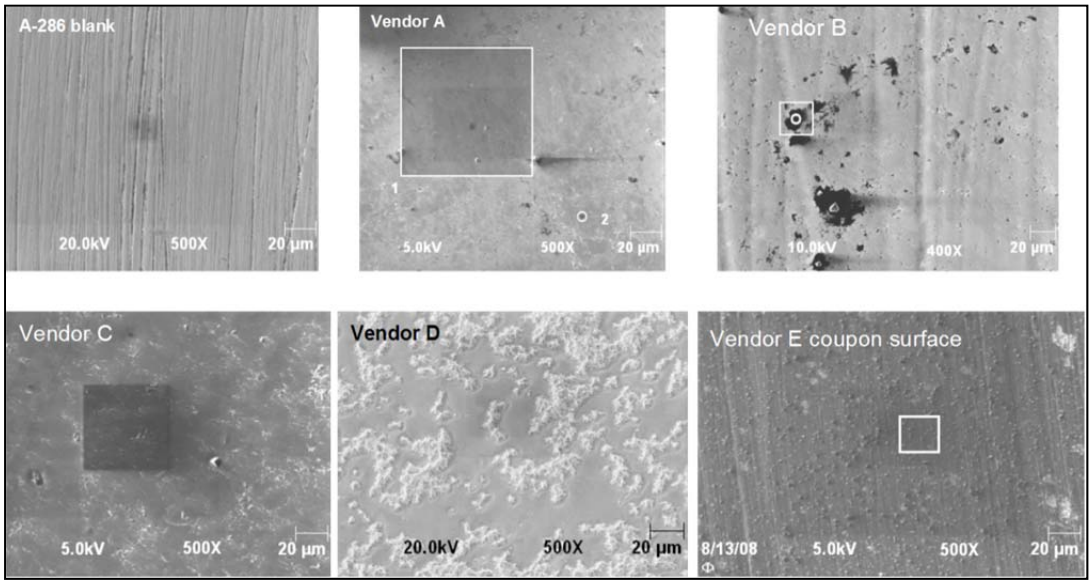

Fig. 1. Scanning electron microscope (SEM) images of untreated stainless steel coupon, and Vendor A-E coupons.

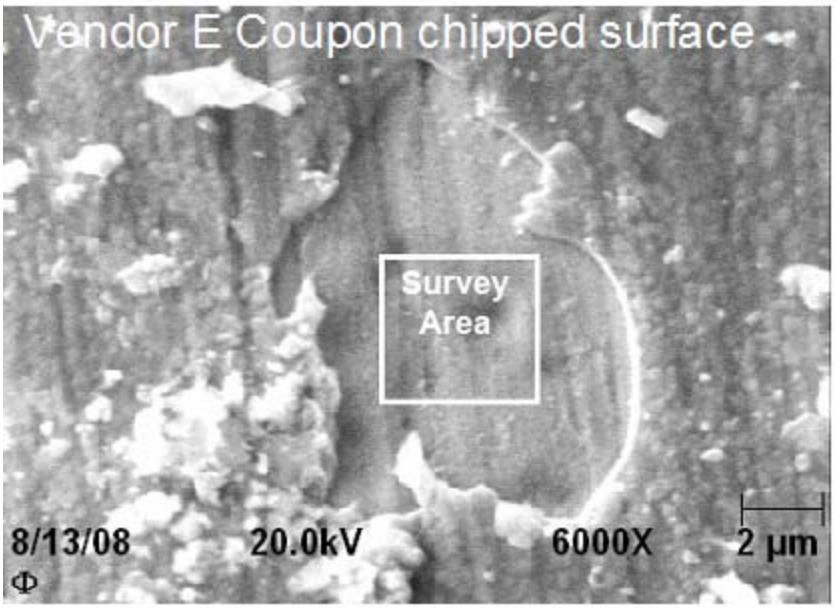

Fig. 2. Scanning electron microscope (SEM) image of Vendor E coupon showing chipped surface.

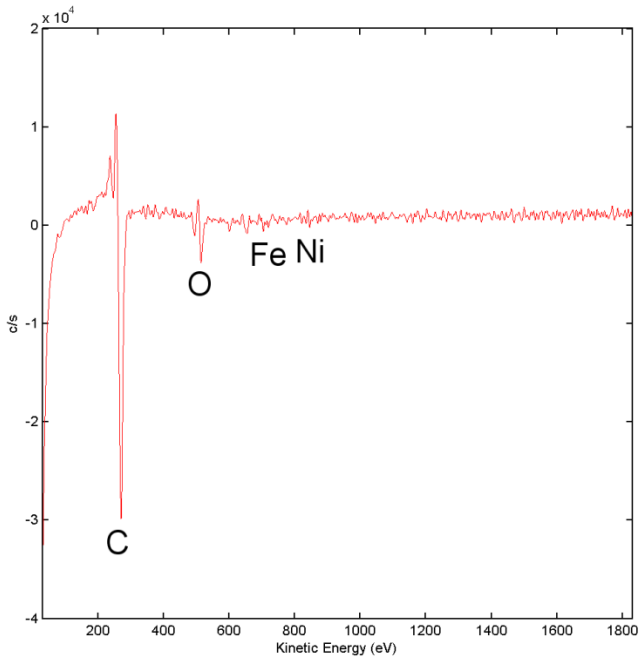

Fig. 3. Auger electron spectroscopy (AES) survey of the untreated stainless steel surface.

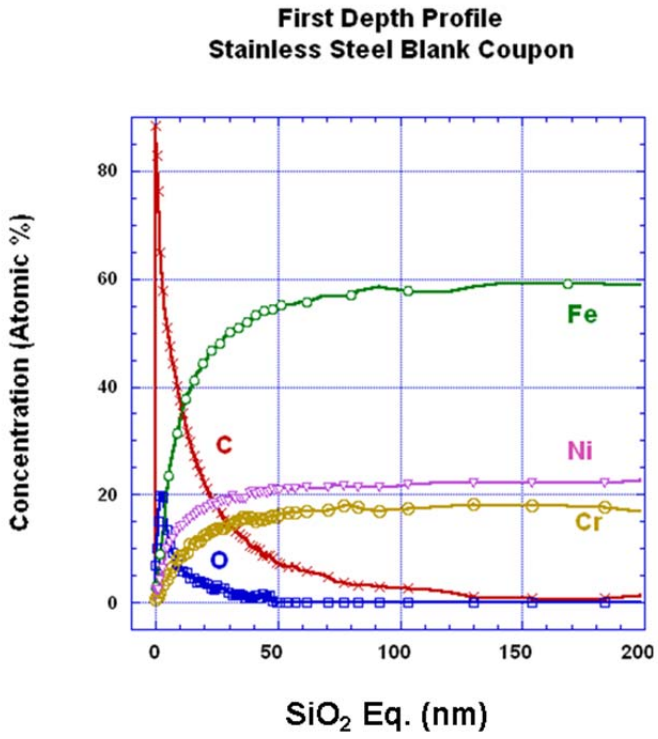

Fig. 4. Auger electron spectroscopy (AES) depth profile of stainless steel blank.

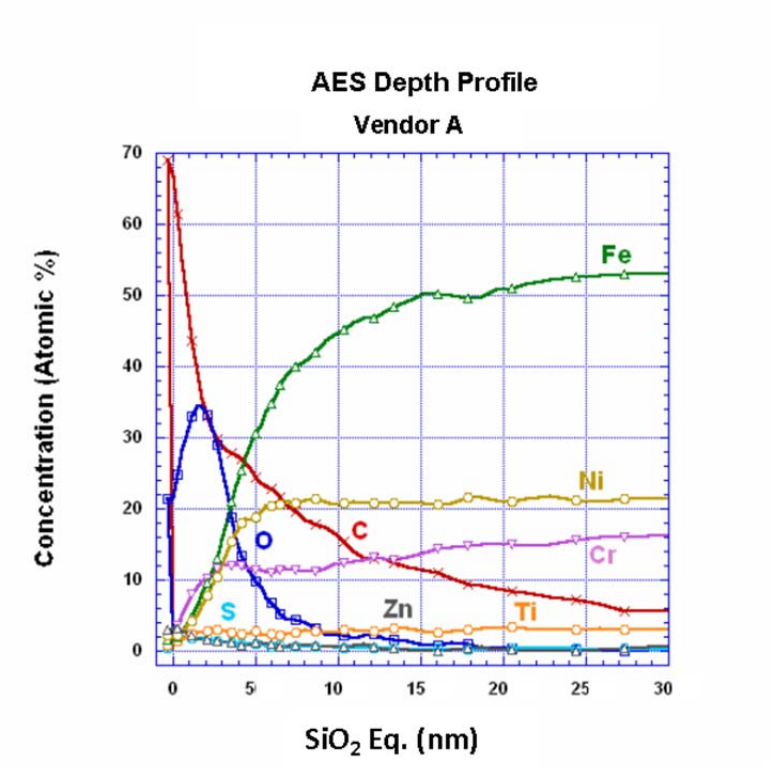

Fig. 5. Auger electron spectroscopy (AES) depth profile of Vendor A treatment.

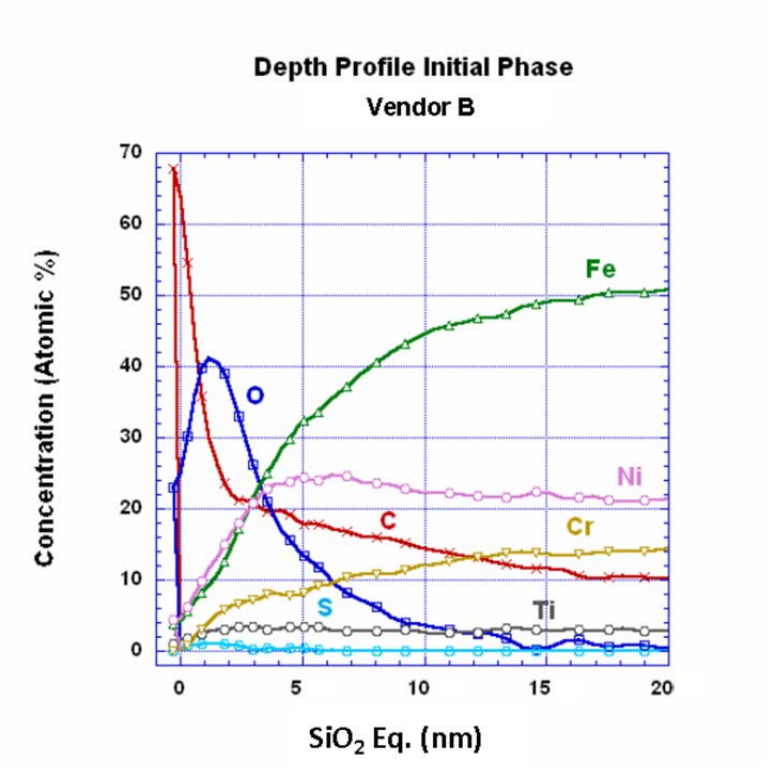

Fig. 6. Auger electron spectroscopy (AES) depth profile of Vendor B coupon.

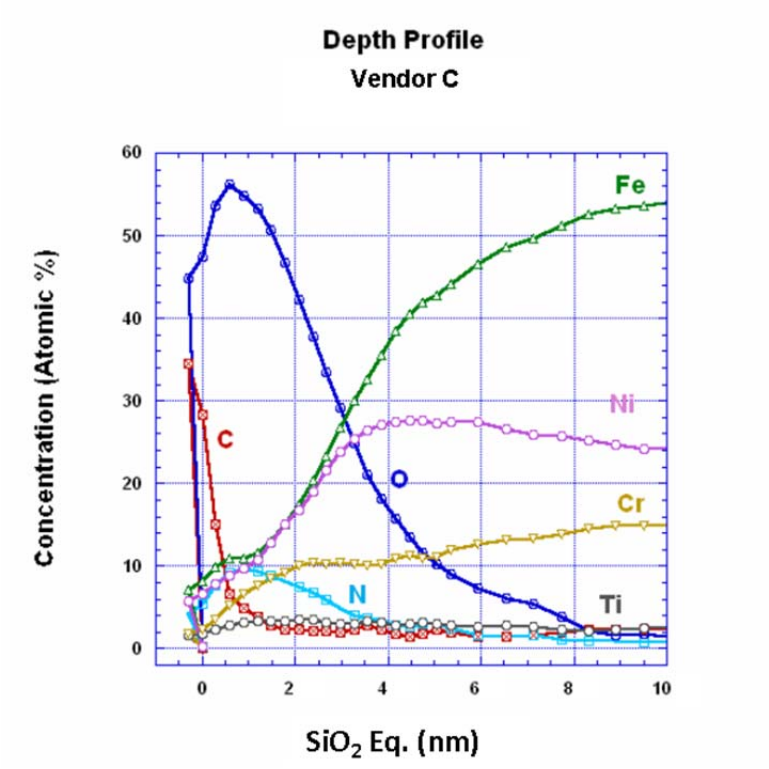

Fig. 7. Auger electron spectroscopy (AES) depth profile of Vendor C coupon.

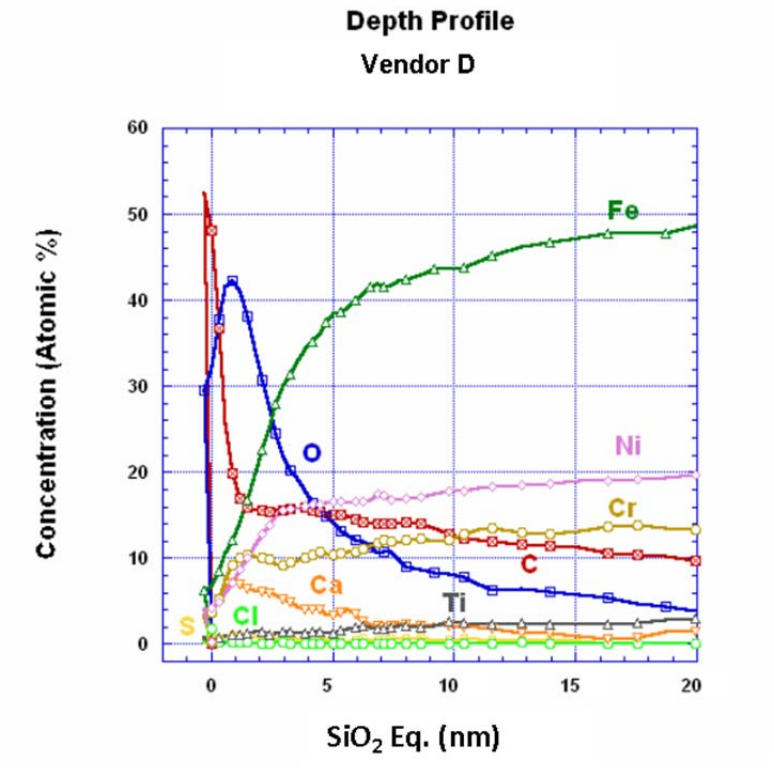

Fig. 8. Auger electron spectroscopy (AES) depth profile of coupon treated by Vendor D.

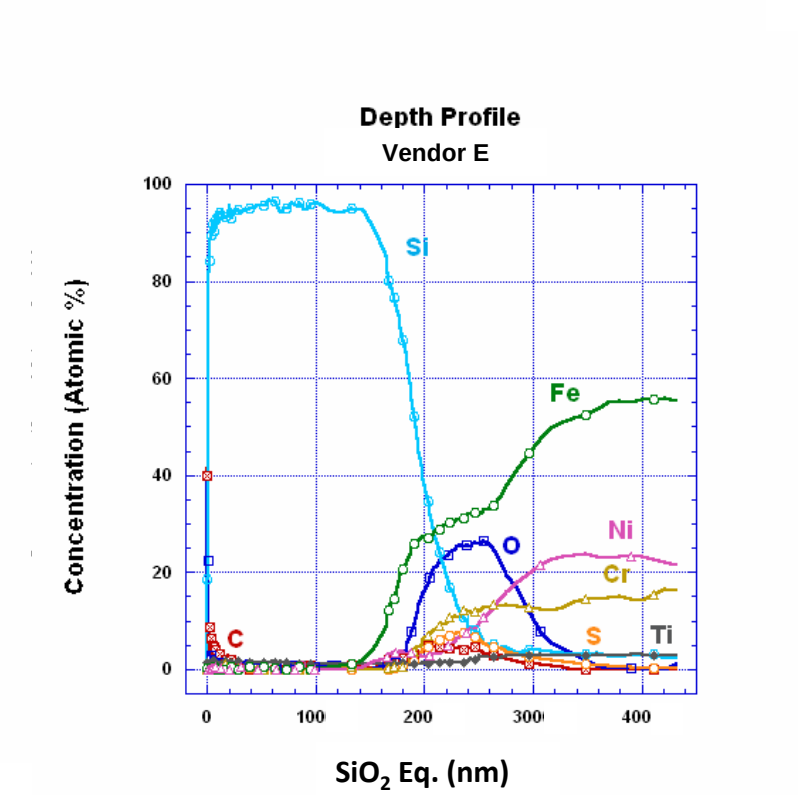

Fig. 9. Auger electron spectroscopy (AES) depth profile of coupon treated by Vendor E.

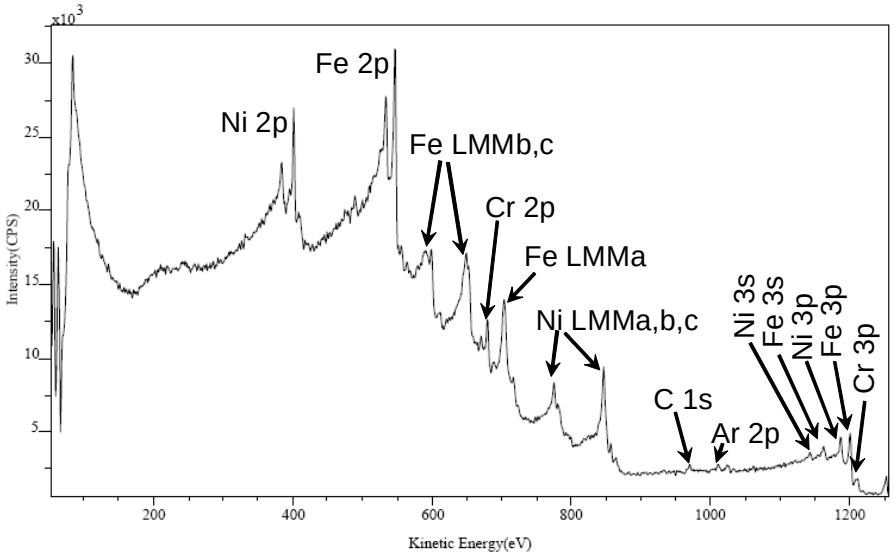

Fig. 10. X-ray photoelectron spectroscopy (XPS) survey of Vendor C coupon sputtered down to bulk stainless steel.

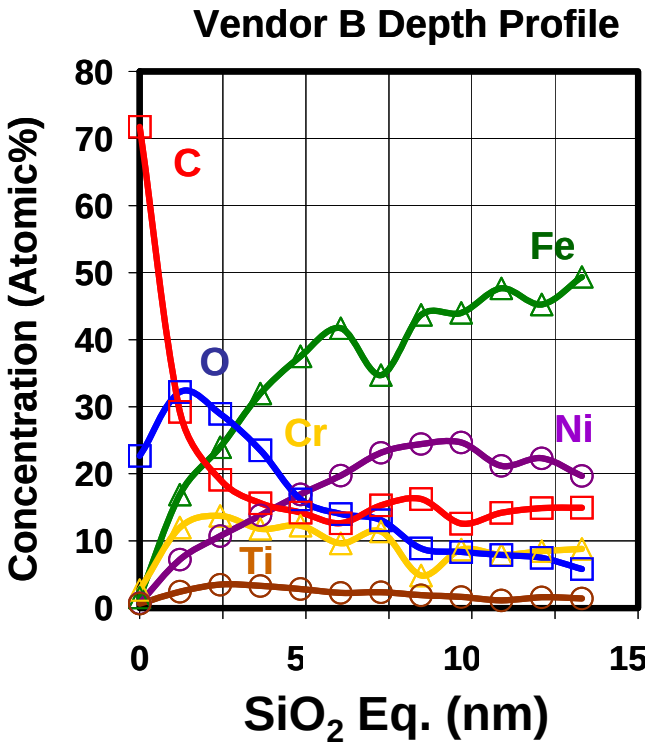

Fig. 11. X-ray photoelectron spectroscopy (XPS) depth profile of Vendor B treatment.

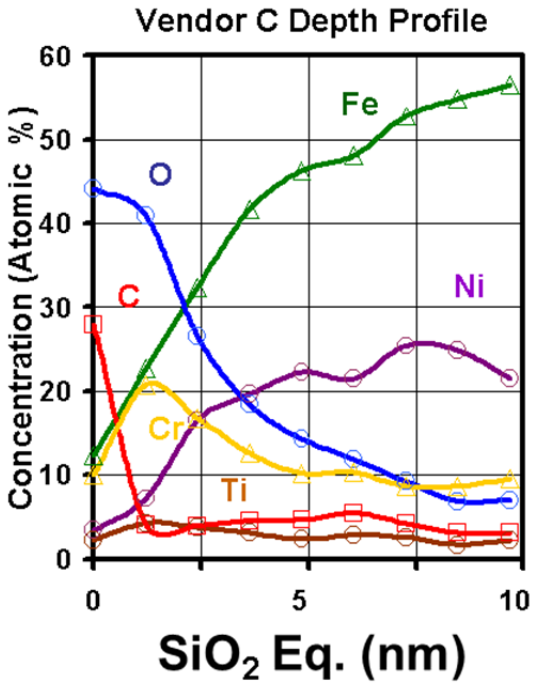

Fig. 12. X-ray photoelectron spectroscopy (XPS) depth profile of Vendor C treatment.

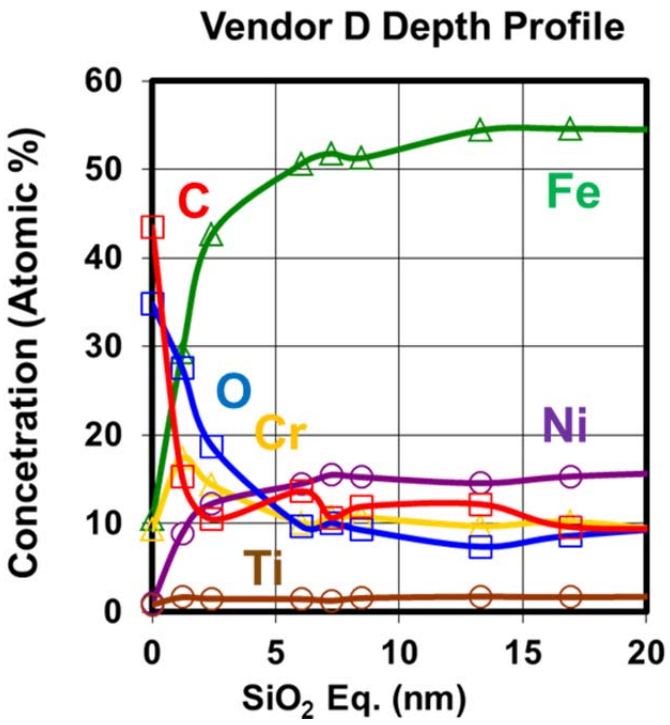

Fig. 13. X-ray photoelectron spectroscopy (XPS) depth profile of Vendor D treatment.

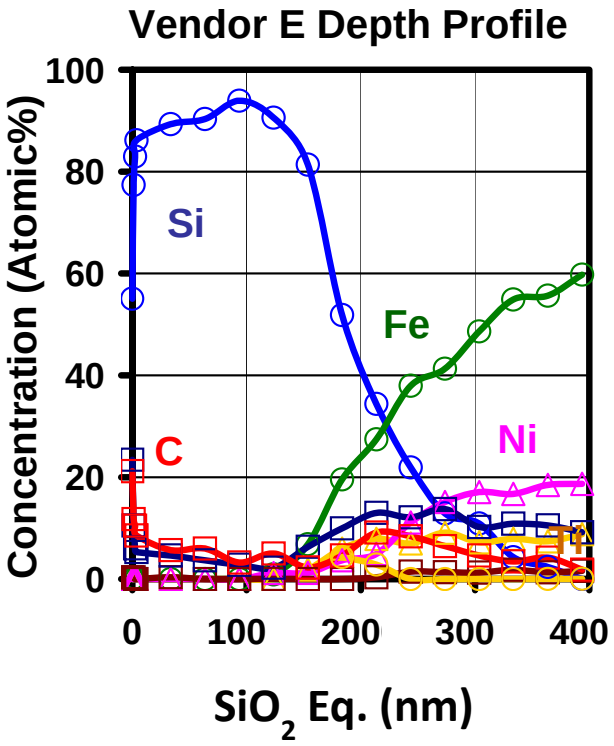

Fig. 14. X-ray photoelectron spectroscopy (XPS) depth profile of Vendor E treatment.

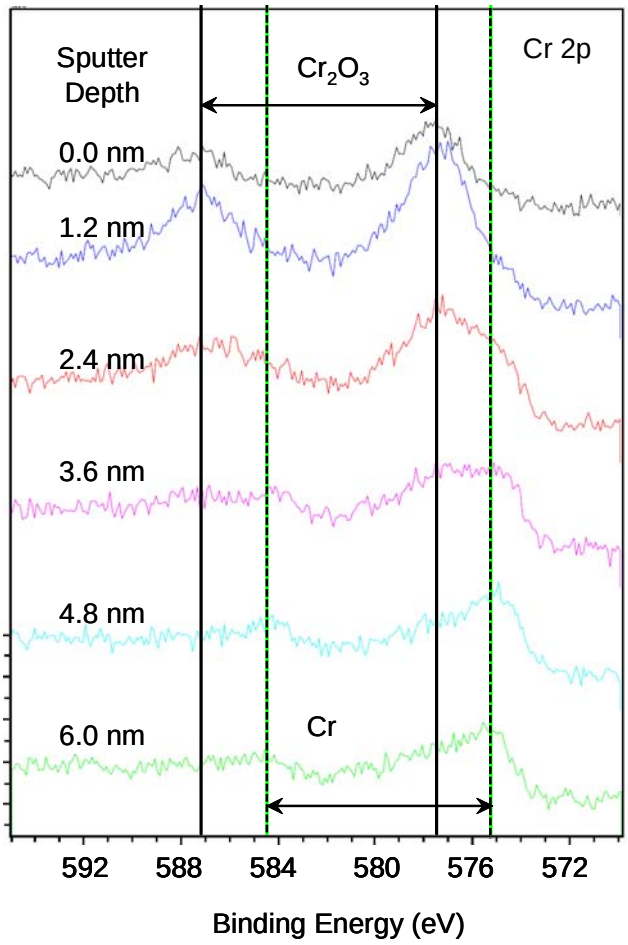

Fig. 15. X-ray photoelectron spectroscopy (XPS) depth profile of Vendor treated coupon showing change from Cr_2O_3 to Cr metal (black lines denote energy of Cr_2O_3 peaks, and dashed green lines energy of Cr metal peaks).